Proceedings of the ASME 2018 1st International Offshore Wind Technical Conference
IOWTC2018
November 4-7, 2018, San Francisco, CA

IOWTC2018-1047

SNAP LOAD CRITERIA FOR MOORING LINES OF A FLOATING OFFSHORE WIND TURBINE

Wei-Ting Hsu[1]
Department of Mechanical Engineering,
University of Maine,
Orono, ME 04469

Krish P. Thiagarajan
Department of Mechanical and Industrial Engineering,
University of Massachusetts Amherst,
Amherst, MA 01003

Lance Manuel
Department of Civil, Architectural, and Environmental Engineering,
The University of Texas At Austin,
Austin, TX 78712

ABSTRACT

There are several challenges facing the design of mooring system of floating offshore wind turbines (FOWTs), including installation costs, stability of lightweight minimalistic platforms, and shallow water depths (50-300m). For station keeping of FOWTs, a proper mooring system is required in order to maintain the translational motions in surge and sway and the rotational motions in yaw of the platform within an adequate range. A combination of light pre-tension, shallow water depth and large platform motions in response to a survival storm condition can result in snap-type impact events on mooring lines, thus increasing the line tension dramatically.

In this paper, we present a new snap load criterion applicable to a catenary mooring system and compare it with Det Norske Veritas' criterion for marine operations. As a case study, we examine the extreme tension on a catenary mooring system of a semi-submersible FOWT exposed to a 100-year storm condition. The software OrcaFlex was used for numerical simulations of the mooring system. NREL's FAST software was coupled to OrcaFlex to obtain aerodynamic loads along with hydrodynamic loads for FOWT analyses. Snap-type impact events were observed in the numerical simulations and were characterized by two criteria. Tension maxima were fitted using composite Weibull distributions (CWDs) and comparisons of probability exceedance were made for the two different snap load criteria.

INTRODUCTION

For station keeping of FOWTs, a proper mooring system is required to keep the translational motions in surge and sway and the rotational motions in yaw of the platform within an adequate range. Common mooring concepts include semi-taut and catenary systems. The catenary refers to the shape that a free hanging line with distributed mass assumes under the influence of gravity. The catenary system provides restoring forces through the suspended weight of the mooring lines and changes in configuration arising from platform motions. A semi-taut leg system usually has an angle of 30 to 45 degrees (to a horizontal plane), and the restoring forces result from axial elastic stretching of the mooring line rather than geometry changes.

A moored floating offshore wind turbine is exposed to various environmental loads, including those arising from wind, waves, and current, acting on the system. The response is affected by a combination of added mass forces, wave drift damping forces, viscous forces, restoring forces and mooring line damping forces. Accounting for all these elements of excitation and response, mooring line tensions can be organized into two components: static and dynamic loads. The static (strictly it should be called quasi-static) mooring line tension is due to the line pretension and mean environmental loads. The dynamic mooring line tension includes low-frequency loads due to platform drift motions and wave-frequency loads due to first-order wave loads.

The design philosophy for offshore structures and moorings is based on principles and practices adopted by the offshore oil

[1] Current Affiliation: Energo Engineering, a KBR company, Houston, TX, 77002

and gas (O&G) industry, and these are optimized for applications in deeper waters (water depth > 400m). In deeper waters, a floating platform's response largely filters the wave frequency forces thus leaving the mooring system to withstand the low-frequency drift forces. The mooring system of a FOWT on the other hand experiences significant effects of wave-frequency forces related to the motions of a light displacement platform in shallow water. Thus FOWT mooring systems may be able to draw upon experience from the O&G industry in designing shallow water Catenary Anchor Leg Mooring (CALM) systems. However, the design principles for CALM systems appear to be proprietary and are not available in the public domain. An FOWT mooring system must be developed by careful consideration of cost, the stability of lightweight minimal platforms (1,000 – 14,000t), and applications for relatively shallow water depths (50 – 500m). The US Department of Energy (DOE) cost of energy models indicate that if platform costs can be held to near 25% of the total system capital cost, then a cost goal of $0.05/kWh would be attainable [1].

When exposed to wave-induced motions, one particular loading condition a FOWT mooring system may be vulnerable to is a snap type impact. A snap load is defined as a spike in tension as a mooring line re-engages immediately following a slack condition; the snap event is typically of very short duration. Therefore, the mooring system of a FOWT may operate in alternating slack-taut conditions, which could cause a discontinuity in the elastic stiffness. Within the duration over which the line becomes taut, the transition from slack to taut condition can cause a snap load which is usually 2 – 3 times the cyclic tension amplitude. Such an impact can result in a shock on the line material leading to immediate failure or considerably reduced service life [2-7]. Hence design practices strongly recommend that this condition be avoided by altering the pre-tension, line length or system make-up.

Although rare, snap events have been documented in marine operations onboard floating platforms, such as the Navion Saga Floating, Storage and Offloading (FSO) vessel and ships used in recovery efforts. Although there have been a very limited number of studies on shock loads on mooring lines of FOWTs [8], there are several investigations on other marine systems such as vertical hanging segmented cable systems [9], lifting and mooring cable systems[3], offshore cranes [20], lines for U.S. Navy ship use [11], marine cable systems [4, 12, 13], multi-cable hoisting systems [14], a Catenary Anchor Leg Mooring (CALM) buoy [15], a deep-sea tethered remotely operated vehicle [16, 17], and a submerged floating tunnel [18]. Some of these studies have investigated the causes and consequences of snap loads on mooring lines of different floating systems. However, no specific criteria for catenary mooring systems are known to exist in a form applicable to FOWTs.

A snap-induced impact on a mooring line may become a dominant problem for the offshore wind power industry. Masciola et al. [8] have studied the influence of mooring line dynamics on the response of a floating offshore wind turbine and compared the results to an equivalent uncoupled mooring model. Snap events were observed in 1:50 scale semi-submersible model tests under survival sea states. Masciola et al. found that the delay between a loss of cable tension and a snap load is short, but is important enough to affect the outcome of the results [8]. While it is worth noting that other studies [19, 20] recommend that snap conditions be avoided to the maximum extent possible during operations, no criterion can be effectively applied to filter snap events.

NOMENCLATURE

F_{total}	total tension
F_{st}	static tension
F_{dyn}	dynamic tension
F_{buoy}	buoyancy force
F_{damp}	damping force
F_I	added inertia force
F_d	drag force
T_H	the horizontal force from the cable on the vessel
T_{FL}	the line tension at the fairlead position
T_{cr}	the critical tension
T	dynamic tension [kN]
T^{max}	local maximum dynamic tension [kN]
T^{min}	local minimum dynamic tension [kN]
T^n	dynamic tension not associated with a snap event [kN]
T_{rms}	root-mean-square dynamic tension [kN]
T^s	snap-induced tension [kN]
T_o	pretension of a mooring line ($T_o = 1124$) [kN]
T_ℓ	slack tension ($T_\ell = 10\%\ T_o$) [kN]
$\hat{T}_{tr}$	non-dimensional transition tension
$\hat{T}_{1,2}$	scale parameters of the composite Weibull distribution function of tension
$\mathcal{F}$	cumulative (Weibull) distribution function of tension; cumulative (composite Weibull) distribution function of tension
η	scale parameter of Weibull distribution function
$\beta_{1,2}$	shape parameters of the composite Weibull distribution function of tension
σ_T	standard deviation of combined low- and wave-frequency components of line tension [kN]

SNAP OCCURRENCE CRITERIA

Although the wind power industry is aware of the importance of snap events on mooring systems, there are no criteria for FOWT systems to predict the associated extreme tensions. In this section, we propose a criterion for catenary mooring systems similar to the development of the Det Norske Veritas (DNV) criterion defined for crane wire systems [21]. Although there are physical differences between the two systems, this approach is taken due to lack of similar criteria for catenary systems.

To understand the DNV criterion, let us consider the vertical hanging cable system (Fig. 1) which supports a fully submerged suspended mass $\mathbb{M}$. In Fig. 1, x_1 is the forced motion of the cable on the top driven by external sources (e.g., motions of the installation vessel in a seaway). Also, x_2 is the motion of the mass

(positive downward), while L_C and k are, respectively, the length and stiffness of the cable.

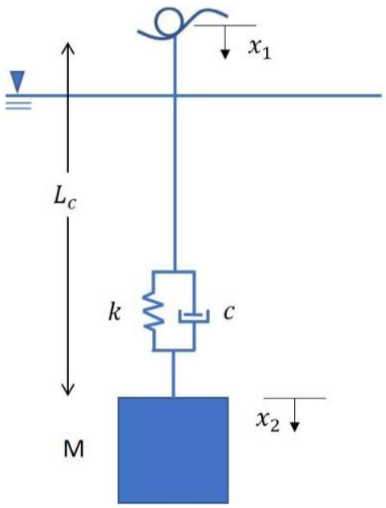

Fig. 1 The vertical hanging cable system

Figure 2 shows a free body diagram of the mass. The forces acting on the mass are fairly well understood, and are described here for completeness. These are:

Buoyancy: $F_{buoy} = \rho_w \forall g$ (1)

Damping: $F_{damp} = C(\dot{x}_2 - \dot{x}_1)$ (2)

Static force: $F_{st} = Mg - \rho_w \forall g$ (3)

Restoring: $F_{dyn} = k(x_2 - x_1)$ (4)

Added inertia: $F_I = \rho_w C_A \forall \ddot{x}_2$ (5)

Drag: $F_d = 0.5\rho_w C_d A_f |\dot{x}_2| \dot{x}_2$ (6)

Here, ρ_w is the water density, A_f and $\forall$ are, respectively, the cross-sectional area and volume of the mass, and C is the internal damping coefficient of the cable. Also, x_2, $\dot{x}_2$, and $\ddot{x}_2$ are, respectively, the displacement, velocity, and acceleration of the mass, while C_d and C_A are, respectively, the drag and added mass coefficients.

Det Norske Veritas (DNV) [21] defines the total line tension in a crane wire as a linear sum of static and dynamic components, i.e.,

$F_{total} = F_{st} + F_{dyn}$ (7)

Here, the static load (F_{st}) is caused by the net effect of the weight lifted by the crane and the changes in buoyancy when the mass enters the water. Noting that the dynamic force (F_{dyn}) can be opposite in direction to the static load, a snap condition is a to occur when the dynamic force exceeds 90% of the static load [21, 22], i.e.

$F_{dyn} > 0.9F_{st}$ (8)

A catenary mooring line provides restoring forces through its suspended weight and the change in configuration that arises from the fairlead motions. A catenary system has a nonlinear restoring force for the surge motion, and is given by Faltinsen [23] as:

$$X = l - h\left(1 + 2\frac{a}{H}\right)^{\frac{1}{2}} + a\cosh^{-1}\left(1 + \frac{H}{a}\right) \quad (9)$$

$$a = \frac{T_H}{w} \quad (10)$$

$$T_{FL} = T_H + wH \quad (11)$$

where X is the horizontal distance from the anchor, H is the water depth, T_{FL} is the line tension at the fairlead position, T_H is the horizontal force from the cable on the vessel and w is the weight per unit length of the mooring line. An example that is used later in this paper is applicable to an FOWT that operates in the water depth of 200m. The weight per unit length of chain in water is 108.7 N/m, and the chain length is 835m. Figure 3 shows the restoring force T_{FL} with respect to horizontal distance X. The dashed tangent lines show the slope of the curve at X_{mean} and X_{max}, which are respectively the mean and maximum surge motion of an FOWT platform during a target operating period. These two tangent lines suggest that the catenary mooring line characteristics approximately resemble a bilinear curve; X_{mean} and X_{max} are selected because there is a strong tendency for the platform to move within the range of these values. While the platform moves from X_{mean} to X_{max} in a short duration during a snap event, it is hypothesized that the mooring line has a higher likelihood of following this bilinear curve than the catenary stiffness curve. The intersection of these two tangent lines is defined as the critical surge motion, X_{cr}, with a corresponding restoring force (T_{cr}). When the platform moves from 0 to X_{cr}, the stiffness is k_{c1}, which then increases to k_{c2} while the platform moves from X_{cr} to X_{max}. Thus, T_{cr} could be an important factor related to the onset of a snap load. Following DNV's approach, let us suppose that a line may snap if the slack tension (T_ℓ) reaches a lower limit of $0.1T_{cr}$. So, for a catenary mooring system, we assume that a snap condition occurs when the dynamic force exceeds 90% of the critical tension, i.e.,

$F_{dyn} > 0.9T_{cr}$ (12)

The two criteria for snap occurrence, Eqs. (8) and (12), are applied to study the exceedance probability of tensions for a semi-submersible FOWT structure. The present study reports on the simulation and probabilistic assessment of snap load frequency and magnitude under these two snap load criteria. State-of-the-art software tools were used to conduct simulations of the semi-submersible platform, including wind turbine dynamics, hydrodynamic platform response, and a fully coupled mooring model.

MODEL AND SOFTWARE DESCRIPTION

The DeepCWind consortium headed by the University of Maine performed model tests of three generic 1:50 scale FOWT concepts – a spar, semi-submersible and a Tension Leg Platform – in MARIN's wave basin facility in the Netherlands in 2011 [24, 25]. The wind turbine model was Froude-scaled based on the National Renewable Energy Laboratory (NREL) 5MW wind turbine. The DeepCWind FOWT models used Froude scaling, and the wind speeds were increased to achieve appropriately

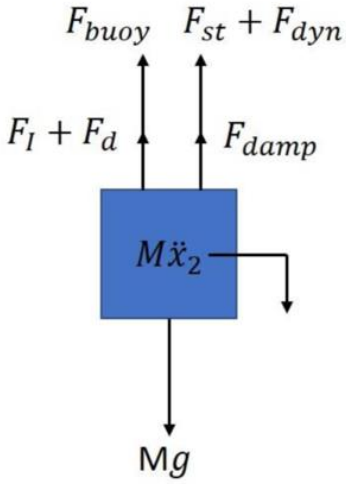

Fig. 2 Free body diagram of the mass-crane wire system

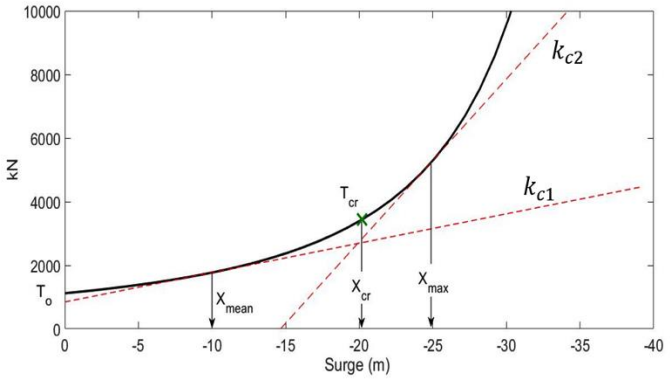

Fig. 3 Sample of the total line tension at the fairlead (T_{FL}) vs. surge motion (X)

scaled thrust forces. The main properties and the model test details can be found in earlier works [24, 25].

The 1:50 scale semi-submersible FOWT studied by the DeepCWind Consortium is used for the analysis. The main properties of the semi-submersible are shown in Table 1. The prototype water depth is 200m and the draft is 20m. The main properties of the NREL 5MW wind turbine are shown in Table 2. The prototype mooring system is up scaled from the model test and includes three catenary lines oriented at 60, 180 and 300 degrees with respect to the x-axis as defined in Fig. 4. The lines are made of stud-less chains with properties as close to standard size chains, and are shown in Table 3. The chosen environment corresponds to a survival sea state described by a JONSWAP spectrum with significant wave height of 10.5m, and mean wave period of 14.3s, acting on the platform for a duration of 3 hours. The encounter direction was set at 180 degrees with respect to the x-axis. Many snap events were observed during the experiments on the mooring chain oriented at 180 degrees with respect to x-axis; thus, the tension data of this mooring line are presented in this paper.

Table 1 Main properties of the semi-submersible platform

Designation	Magnitude	Unit
Mass	14,040	ton
Displacement	14,265	ton
Center of Gravity above keel	10.11	m
Roll radius of gyration in air	31.61	m
Pitch radius of gyration in air	32.34	m
Natural roll period (moored)	26.9	s
Natural pitch period (moored)	26.8	s
Natural heave period (moored)	17.5	s

Table 2 Main properties of the NREL 5MW wind turbine

Designation	Magnitude	Unit
Rotor orientation, configuration	Upwind, 3 blades	
Rotor diameter	126.0	m
Hub diameter	3.0	m
Hub height above SWL	90.0	m
Height of tower-top flange above SWL	87.6	m
Total tower-top mass	397,160	kg

Table 3 Main properties of the mooring line

Designation	Magnitude	Unit
Radius to anchor	837.6	m
Depth of anchor	200	m
Radius to fairlead	40.9	m
Draft of fairlead	14	m
Un-stretched line length	835.5	m
Line diameter	80	mm
Line mass density (dry)	123.8	kg/m
Line mass density (wet)	108.7	kg/m
Line extensional stiffness	752.9	MN

State-of-the-art software tools were used to conduct simulations of the semi-submersible, including wind turbine dynamics, hydrodynamic platform responses, and a fully coupled mooring model. The tools are described briefly here.

Rhino 3D - a commercial 3D computer graphics and computer-aided design (CAD) application software was used to develop the model geometry.

ANSYS AQWA – an engineering analysis suite of tools for the investigation of the effect of waves, wind and current on floating and fixed offshore and marine structures was used. ANSYS AQWA has a time- and frequency-domain boundary element solver for floating bodies in an ocean environment. The mesh and linear hydrodynamic database were developed in this program.

OrcaFlex – a package for the dynamic analysis of offshore marine systems was also used. OrcaFlex includes a time-domain solver to find locations and stresses of flexible elements in an offshore system, including structural and fatigue analysis. This software requires as input, hydrodynamic coefficients of the floating body from an appropriate boundary element solver, e.g., ANSYS AQWA. The second-order difference/sum frequency excitation force calculated by the QTF method was applied. The mooring dynamics were modeled using OrcaFlex with a non-linear finite element model.

FASTLink – a coupler that enables running FAST within the OrcaFlex environment – was used to obtain aerodynamic loads along with hydrodynamic loads for the FOWT analysis. A discussion of the implementation and use of FASTLink is provided by Masciola et al. [26]. Turbine aerodynamic analysis is often conducted using the NREL-FAST code, which has been applied to FOWTs for research, design, and development of government standards. In this paper, we use FAST and OrcaFlex connected by the FASTLink coupler. Extensive validation work using these software has been reported upon in [2].

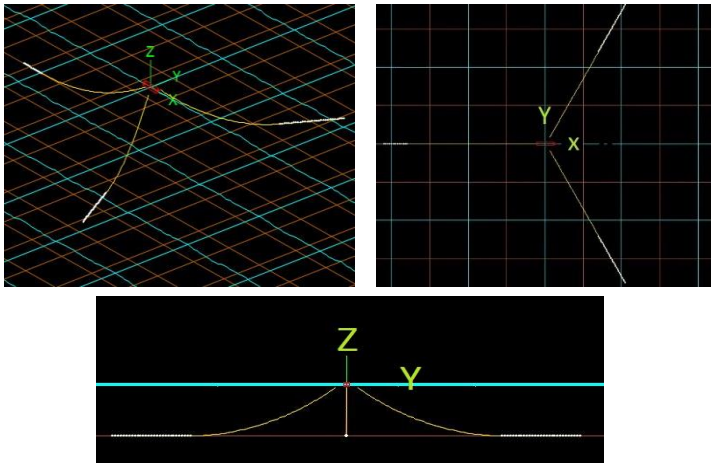

Fig. 4 The semi-submersible platform and wind turbine model set-up in the basin

NUMERICAL PREDICTION OF MOORING TENSION IN A 100-YR STORM

In this study, we present results from seven numerical runs of the semi-submersible FOWT under survival storm conditions (i.e., a 100-year storm). For all these cases, the significant wave height and peak wave period are held constant at 10.5m and 14.3s, respectively, while the wind speed is varied from 0 to 30.5 m/ s, as shown in Table 4. The wind conditions range from a steady wind to turbulent wind described by a chosen spectrum. These values correspond to similar conditions used in experiments.

Figure 5 shows an illustrative time history of the line tension at the fairlead obtained from experiments. For this case, the significant height, peak wave period and steady wind speed were 10.5 m, 14.3 s, and 30.5 m/s, respectively. Applying DNV's criterion, i.e., Eq. (8), a threshold minimum is defined at 10% of the pre-tension value. A snap event is initiated after a local minimum tension value falls below this threshold tension, and it lasts until the tension spikes to a value greater than the pretension.

Table 4. Wave and wind conditions for the numerical runs

Case	Wave Conditions			Wind Conditions		
	H_s (m)	T_p (s)	Γ	V_w (m/s)	Wind Type	Ω (rpm)
1	10.5	14.3	3	0	-	0
2	10.5	14.3	3	21	Turbulent	12.73
3*	10.5	14.3	3	21	Turbulent	12.73
4	10.5	14.3	3	21	Steady	12.73
5*	10.5	14.3	3	21	Steady	12.73
6	10.5	14.3	3	30.5	Turbulent	0
7	10.5	14.3	3	30.5	Steady	0

(* indicates cases with a nacelle yaw error of 20 degrees)

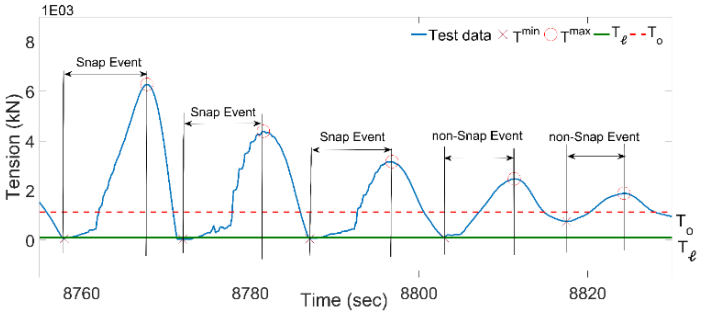

Fig. 5 Demonstration of mooring line time history along with snap events

Consistent with [23], the dynamic tension (T_i) is defined as the range extending from a local minimum to the immediately following maximum (shown in Fig. 5), i.e.,

$$T_i = T_i^{max} - T_i^{min}, i = 1 \; to \; r \tag{13}$$

where r is the total number of measurements of dynamic tension values from a time history. The set of cyclical dynamic tensions are separated into snap-induced dynamic tensions (T^s) and those that are not associated with a snap event (T^n). The latter could be labeled as non-snap events. The distinction between T^n and T^s is based on whether or not the range exceeds the minimum and maximum thresholds, i.e.,

$$T_j^n = T_j^{max} - T_j^{min} \; for \begin{cases} T_j^{max} > T_o \\ T_j^{min} > T_\ell \end{cases}, j = 1 \; to \; p \tag{14}$$

$$T_k^s = T_k^{max} - T_k^{min} \; for \begin{cases} T_k^{max} > T_o \\ T_k^{min} \leq T_\ell \end{cases}, k = 1 \; to \; q \tag{15}$$

Here, T_o is the pretension of the mooring line and T_ℓ is the slack tension defined by Eqs. (8) or (12). The three time series—i.e., T, T^n and T^s—for each 3.5-hour storm test data set are made non-dimensional in the following manner:

$$\hat{T} = T/T_{rms} \tag{16}$$

$$\hat{T}^n = T^n/T_{rms} \quad (17)$$
$$\hat{T}^s = T^s/T_{rms} \quad (18)$$

where T_{rms} represents the root-mean-square (rms) maximum dynamic tension. Henceforth, the non-dimensional dynamic tension is referred to as the dynamic tension for brevity. The tension time series data are made non-dimensional in the following manner:

$$\hat{T}_{dyn}(t) = T_{dyn}(t)/T_{rms} \quad (19)$$
$$\hat{T}_\ell = T_\ell/T_{rms} \quad (20)$$
$$\hat{T}_{cr} = T_{cr}/T_{rms} \quad (21)$$
$$\hat{T}^{min} = T^{min}/T_{rms} \quad (22)$$

where $\hat{T}_\ell$ = 0.34 and 0.12 for the proposed criterion (Eq. 12) and for DNV's criterion (Eq. 8) respectively. Table 5 summarizes data on $\hat{T}$, $\hat{T}^n$ and $\hat{T}^s$ for Case 1 under $\hat{T}_\ell$ = 0.34 and $\hat{T}_\ell$ = 0.12. The snap events increase by a factor of 2.8 when $\hat{T}_\ell$ increases from 0.12 to 0.34. For $\hat{T}_\ell$ = 0.34, the greatest value of $\hat{T}^n$ equals 2.67 which is 28% smaller than that for $\hat{T}_\ell$ = 0.12. The smallest value of $\hat{T}^s$ equals 1.34 which is also 28% smaller than the corresponding value for $\hat{T}_\ell$ = 0.12. Thus, by applying the new criterion to the data, smaller maximum $\hat{T}^n$ values, smaller minimum $\hat{T}^s$ values and an increased number of snap events are observed.

Table 5. Normalized tension ranges, number of cycles, and duration of $\hat{T}$, $\hat{T}^n$ and $\hat{T}^s$ in Case 1 for $\hat{T}_\ell$ =0.34 (Eq. 12) and $\hat{T}_\ell$=0.12 (Eq. 8)

$\hat{T}_\ell$	$\hat{T}$		$\hat{T}^n$			$\hat{T}^s$		
	Tension range	# cycles	Tension range		# cycles	Duration range (sec / cycle)	Tension range	
	Min Max		Min Max				Min	Max
0.34	0.10 -	4.25	873	0.10 - 2.67	61	5.4 - 10.6	1.34 -	4.25
0.12	0.10 -	4.25	912	0.10 - 3.70	22	6.2 - 10.2	1.85 -	4.25

EXCEEDANCE PROBABILITY OF TENSION MAXIMA

Exceedance probability (P) estimates are commonly used for characterizing the probability that a variable of interest exceeds any specified threshold value. Following Hsu et al. [27], for a threshold value, $\hat{T}_j$, the exceedance probability of a line's dynamic tension, $\hat{T}$, in a given sample is given as:

$$\mathrm{P}(\hat{T}_j) = \mathrm{P}[\hat{T} > \hat{T}_j] = 1 - n_j/(r+1) \quad (23)$$

where r is the total number of values of $\hat{T}$, and n_j is the number of tension values that exceed the threshold. Figure 6 compares the exceedance probabilities of the dynamic tension ($\hat{T}$) for the stationary rotor, i.e., steady wind Case 1, evaluated by the two criteria. The snap and non-snap data are indicated by open and closed symbols, respectively. Beyond the transition range, the exceedance probability curve is contributed to by $\hat{T}^s$ for $\hat{T}_\ell$ = 0.34, while for $\hat{T}_\ell$ = 0.12, there is still some overlap of tension values from non-snap and snap events. In Fig. 6, there is a tendency of the cyclical dynamic tension with $\hat{T}^{min}$ ranging from 0.12 to 0.34 to occur with a tension range of 2 to 3.7. For $\hat{T}_\ell$ = 0.12, most of the snap events are also observed in this tension range of 2 – 3.7. This indicates that cyclical dynamic tension, which has similar tension values with snap events, may be ignored by using DNV's criterion.

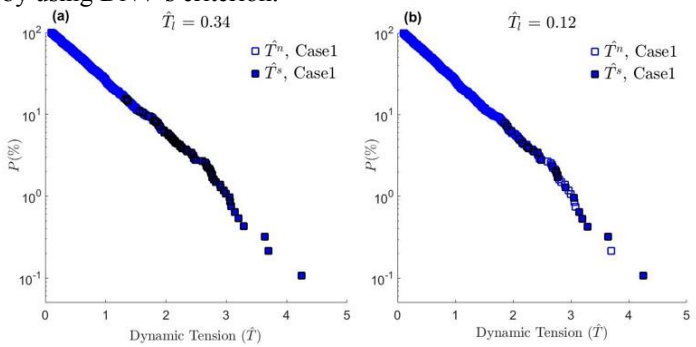

Fig. 6. A comparison of exceedance probability curves for $\hat{T}^n$ (hollow markers) and $\hat{T}^s$ (solid markers) for two cases: (a) $\hat{T}_\ell$ = 0.34, and (b) $\hat{T}_\ell$ = 0.12

We further analyze the non-snap tensions using a Weibull (WBL) model. Following [27], the WBL cumulative distribution function is given by

$$\mathcal{F}(\hat{T}) = 1 - \exp\left[-\left(\frac{\hat{T}}{\eta}\right)^{\xi}\right] \text{ for } \hat{T} \geq 0, \text{ and } \eta, \xi \in \mathbb{R}. \quad (24)$$

where η and ξ (both greater than zero) are the so-called scale and shape parameters, respectively. The method of Maximum Likelihood Estimation (MLE) is applied to estimate the WBL model parameters, η and ξ [27]. In Fig. 7, the exceedance probability plot of $\hat{T}^n$ deviates considerably from the probability of $\hat{T}$ beyond the lower tension range and falls more steeply in the tension range of 2.6 – 2.8 when compared with $\hat{T}_\ell$ = 0.12. For $\hat{T}_\ell$ = 0.12, the largest value of n is 3.7, which is in the higher tension range. When compared with $\hat{T}_\ell$ = 0.12, $\hat{T}^n$of FASTLink suggests larger right-tail probability levels.

In Table 6, the value of the WBL shape parameter (ξ) estimated for $\hat{T}^n$ when $\hat{T}_\ell$ = 0.34 is larger than the value obtained for $\hat{T}_\ell$ = 0.12. Thus, $\hat{T}^n$ exhibits smaller right probability tail levels under $\hat{T}_\ell$ = 0.34 when compared to those of $\hat{T}_\ell$ = 0.12. For $\hat{T}_\ell$ = 0.34, the distribution of $\hat{T}^n$ is well represented by a Weibull model (Fig. 7). For $\hat{T}_\ell$ = 0.12, $\hat{T}^n$has heavier right probability tail levels and is not fitted well by the WBL model (Fig. 7). Figure 7 shows evidence that the T_n data might include cyclic dynamic tensions that have similar characteristics to the snap events under $\hat{T}_\ell$ = 0.12. Figure 8 shows that the WBL model does not fit the $\hat{T}^s$ data very well for larger tension ranges of $\hat{T}_\ell$ = 0.34, when compared to the one for $\hat{T}_\ell$ = 0.12.

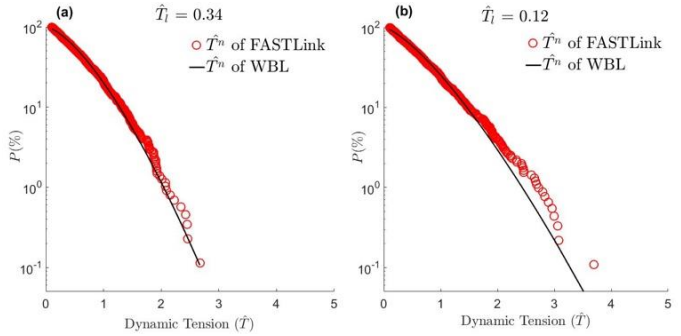

Fig. 7. A comparison of exceedance probability curves for $\hat{T}^n$ between FASTLink (hollow circles) and WBL (solid line) for: (a) $\hat{T}_\ell$ = 0.34, and (b) $\hat{T}_\ell$ = 0.12

Table 6. Scale (η) and shape (ξ) parameters for WBL distributions fitted to $\hat{T}$, $\hat{T}^n$and $\hat{T}^s$ for $\hat{T}_\ell$ = 0.34 and $\hat{T}_\ell$ = 0.12

$\hat{T}_\ell$	$\hat{T}$		$\hat{T}^n$		$\hat{T}^s$	
	Scale (η)	Shape (ξ)	Scale (η)	Shape (ξ)	Scale (η)	Shape (ξ)
0.34	0.835	1.296	0.726	1.477	2.623	4.143
0.12	0.835	1.296	0.792	1.360	2.916	4.654

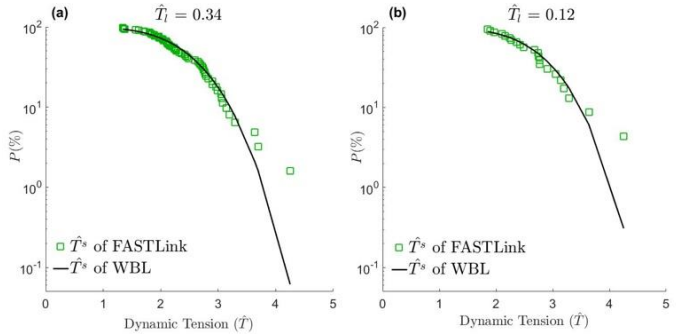

Fig. 8. A comparison of exceedance probability curves for $\hat{T}^s$ between FASTLink (hollow circles) and WBL (solid line) for: (a) $\hat{T}_\ell$ = 0.34, and (b) $\hat{T}_\ell$ = 0.12

The study by Hsu et al. [27] presented a composite Weibull distribution (CWD) model applied to the non-dimensional dynamic tension ($\hat{T}$):

$$\mathcal{F}(\hat{T}) = \begin{cases} \mathcal{F}_1(\hat{T}) = 1 - \exp\left[-(\hat{T}/\hat{T}_1)^{\beta_1}\right], \ \hat{T} \le \hat{T}_{tr} \\ \mathcal{F}_2(\hat{T}) = 1 - \exp\left[-(\hat{T}/\hat{T}_2)^{\beta_2}\right], \ \hat{T} \ge \hat{T}_{tr} \end{cases} \quad (25)$$

Here $\mathcal{F}(\hat{T})$ is the cumulative composite Weibull probability distribution of $\hat{T}$; also, β_1, β_2 are the shape parameters and $\hat{T}_1, \hat{T}_2$ are the scale parameters. The transition tension ($\hat{T}_{tr}$) is the value at which the tension values switch from non-snap to snap tensions; this value is closely related to the maximum tension predicted by using the non-snap values alone [27], i.e.,

$$\hat{T}_{tr} = \delta \cdot 2(\sigma_T\sqrt{2\ln N_T})/T_{rms} \quad (26)$$

where N_T is the number of combined low- and wave-frequency platform oscillations over the duration of the environmental sea state under consideration. For the seven cases under consideration, N_T equals 881 corresponding to a peak period of 14.3 s and a 3.5-hour duration. Based on the two snap criteria, the transition tensions are evaluated as shown in Table 7. Figure 9 shows the CWD model comparison between $\hat{T}_{tr}$ = 3.7 and $\hat{T}_{tr}$ = 2.62. It is obvious that, for $\hat{T}_{tr}$ = 3.7, the dynamic tension is not well described by the CWD model for the larger tension ranges. The most probable maximum estimate (MPME) of the dynamic tension based on the CWD model is [27]:

$$\hat{T}_{MPME} = \hat{T}_2[\ln(r)]^{1/\beta_2} \quad (27)$$

These values are evaluated for the two distributions and are shown in Table 7. The maximum tensions obtained by including snap tensions using the two criteria are similar in magnitude, differing by less than 5%.

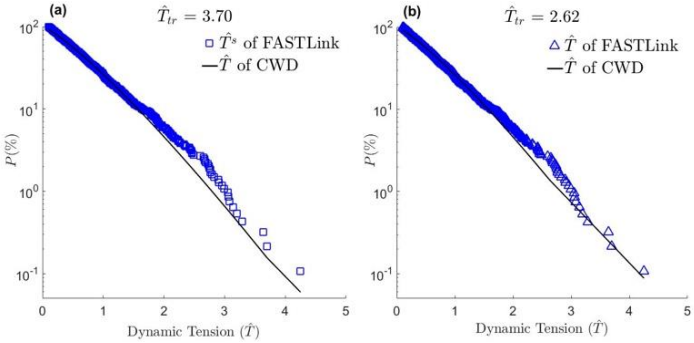

Fig. 9. A comparison of exceedance probability curves for $\hat{T}$ between FASTLink (hollow circles) and CWD (solid line) for: (a) $\hat{T}_{tr}$ = 3.70, and (b) $\hat{T}_{tr}$ = 2.62

Table 7Error! No text of specified style in document.. The shape parameters (β_1; β_2) and scale parameters ($\hat{T}_1$; $\hat{T}_2$) for the CWD for $\hat{T}_{tr}$ = 3.70 and $\hat{T}_{tr}$ = 2.62

$\hat{T}_\ell$	$\hat{T}_{tr}$	$\hat{T}_1$	β_1	$\hat{T}_2$	β_2	$\hat{T}_{MPME}$
0.34	3.70	0.786	1.205	0.568	0.996	3.91
0.12	2.62	0.786	1.205	0.642	1.032	4.14

CONCLUSIONS

In this paper, we presented a new snap load criterion applicable to a catenary mooring system and compared it with the well-known criterion proposed by Det Norske Veritas for marine operations. As a case study, we examined the extreme tension on a catenary mooring system of a semi-submersible FOWT exposed to a 100-year storm condition. The software OrcaFlex combined with NREL's FAST software was used for numerical simulations of the mooring system. Snap-type impact events were observed in the numerical simulation and were characterized by the two

criteria. Tension maxima were fitted using composite Weibull distributions (CWDs) and comparisons of exceedance probability were made for the two different snap load criteria. The maximum tension values predicted using the two approaches were slightly different, only by about 5%. The approach demonstrates the robustness of the proposed snap criterion for catenary moored systems.

It is important that snap load criteria be further validated. The ad hoc nature of the snap criterion could be further studied by conducting sensitivity tests on the 10% safety margin proposed in Eq. (12). The environmental conditions in Table 4 mimicked those used in previous experimental and computational studies. Future work could involve different sea states incorporating effects such as current flows. Once the robustness of the snap criterion has been established, it can be used to identify snap events when they occur in simulations or in practice. Alternatively, due to the higher probabilities of exceedance, FOWT mooring systems may be designed to withstand such loads by incorporating a higher safety factor.

ACKNOWLEDGMENTS

Access to the OrcaFlex software used in the simulations was provided by Maine Marine Composites, LLC. Portland, ME.

REFERENCES

[1] Musial W, Butterfield S, Boone A. Feasibility of Floating Platform Systems for Wind Turbines. 23rd ASME Wind Energy Symposium. Reno, Nevada 2004.

[2] Hsu W-T, Thiagarajan KP, MacNicoll M, Akers R. Prediction of Extreme Tensions in Mooring Lines of a Floating Offshore Wind Turbine in a 100-Year Storm. Proceedings of the ASME 2015 34th International Conference on Ocean, Offshore and Arctic Engineering. St. John's, NL, Canada: ASME; 2015.

[3] Liu FC. Snap Loads and Bending Fatigue in Diving Bell Handling Systems. Offshore Technology Conference. Houston,TX1981.

[4] Niedzwecki JM, Thampi SK. Snap Loading of Marine Cable Systems. Applied Ocean Research. 1991;13:210-9.

[5] Salancy AM, Bea RG. Offshore Single Point Mooring Systems for Import of Hazardous Liquid Cargoes Offshore Southern California. International Society of Offshore and Polar Engineers. Honolulu, USA: International Society of Offshore and Polar Engineers; 1997.

[6] Shah AA, Umar A, Siddiqui NA. A Methodology for Assessing the Reliability of Taut and Slack Mooring Systems against Instability. Ocean Engineering. 2005;32:1216-34.

[7] Gobat JI, Grosenbaugh MA. Dynamics in the Touchdown Region of Catenary Moorings. The Eleventh (2001) International Offshore and Polar Engineering Conference. Stavanger, Norway2001. p. 273-81.

[8] Masciola M, Robertson A, Jonkman J, Coulling A, Goupee A. Assessment of the Importance of Mooring Dynamics on the Global Response of the Deepcwind Floating Semisubmersible Offshore Wind Turbine. The Twenty-third (2013) International Offshore and Polar Engineering. Anchorage, Alaska, USA2013. p. 359-68.

[9] Goeller JE, Laura PA. Analytical and Experimental Study of the Dynamic Response of Segmented Cable Systems. Journal of Sound and Vibration. 1971;18:311-24.

[10] Strengehagen J, Gran S. Supply Boat Motion, Dynamic Response and Fatigue of Offshore Cranes. Offshore Technology Conference. Houston, TX, USA1980.

[11] Swenson RC. A Snap-Back Restrained Kevlar Mooring Line. Offshore Technology Conference. Houston, TX, UAS1983.

[12] Huang S, Vassalos D. A Numerical Method for Predicting Snap Loading of Marine Cables. Applied Ocean Research. 1993;15:235-42.

[13] Han JS, Son Y-J, Choi HS, Rho JB. The Transient Behavior of Mooring Systems in Line-Broken Condition. The Twenty-first (2011) International Offshore and Polar Engineering Conference. Maui, Hawaii, USA: International Society of Offshore and Polar Engineers; 2011.

[14] Hann M. Statics and Dynamics of Multi-Cable Systems for Submersibles. Marine Structures. 1995;8:555-83.

[15] Cozijn IJL, Bunnik ITHJ. Omae2004-51370. 23rd International Conference on Offshore Mechanics and Arctic Engineering. Vancouver, Canada2004. p. 1-11.

[16] Zhu K-q, Zhu H-y, Zhang Y-s, Gao J, Miao G-p. A Multi-Body Space-Coupled Motion Simulation for a Deep-Sea Tethered Remotely Operated Vehicle. Journal of Hydrodynamics, Ser B. 2008;20:210-5.

[17] Zhu K-q, Zheng D-c, Cai Y, Yu C-l, Wang R, Liu Y-l, Zhang F. Nonlinear Hydrodynamic Response of Marine Cable -Body System under Random Dynamic Excitations. Journal of Hydrodynamics, Ser B. 2009;21:851-5.

[18] Lu W, Ge F, Wang L, Wu X, Hong Y. On the Slack Phenomena and Snap Force in Tethers of Submerged Floating Tunnels under Wave Conditions. Marine Structures. 2011;24:358-76.

[19] Gerber M, Engelbrecht L. The Bilinear Oscillator: The Response of an Articulated Mooring Tower Driven by Irregular Seas. Ocean Engineering. 1993;20:113-33.

[20] Brommundt M, Krause L, Merz K, Muskulus M. Mooring System Optimization for Floating Wind Turbines Using Frequency Domain Analysis. Energy Procedia. 2012;24:289-96.

[21] DNV. Rules for Planning and Execution of Marine Operations. Hovik, Norway: Det Norske Veritas; 1996.

[22] DNV. Modeling and Analysis of Marine Operations. Recommended Practice DNV-RP-H103. Hovik, Norway: DET NORSKE VERITAS; 2011.

[23] Faltinsen OM. Sea Loads on Ships and Offshore Structures. United Kingdom: The Press Syndicate of the University of Cambridge; 1998.

[24] Kimball RW, Goupee AJ, Coulling AJ, Dagher HJ. Model Test Comparisons of TLP, Spar-Buoy and Semisubmersible Floating Offshore Wind Turbine Systems. Proceedings SNAME Annual Meeting. 2012.

[25] Koo B, Goupee AJ, Lambrakos K, Kimball RW. Model Tests for a Floating Windturbine on Three Different Floaters. ASME 2012 31st International Conference on Ocean, Offshore and Arctic Engineering. Rio de Janeiro, Brazil. 2012. p. 455-65.

[26] Masciola M, Robertson A, Jonkman J, Driscoll FR. Investigation of a FAST-Orcaflex Coupling Module for Integrating Turbine and Mooring Dynamics of Offshore Floating Wind Turbines. International Conference on Offshore Wind Energy and Ocean Energy. Beijing, China. 2011. p. NREL/CP-5000-52896.
[27] Hsu, W. T., Thiagarajan, K. P., Manuel, L., (2017) Extreme mooring tensions due to snap loads on a floating offshore wind turbine system, Marine Str. 55 (September 2017), pp. 182 – 199.
[28] Rinne H. The Weibull Distribution: A Handbook. Boca Raton: CRC Press; 2009